210

CONTROLLED HIGH-RATE DEFORMATION OF Ti-GRAPHITE and Ti-ULTRAFINE DIAMOND MIXTURES

H.C. Chen, V.F. Nesterenko, and M.A. Meyers

Department of Applied Mechanics and Engineering Sciences

University of California, San Diego

La Jolla, CA 92093

ABSTRACT

Ti-C powder mixtures were subjected to high - strain - rate deformation in an experimental setup through the dynamic radial collapse of a thick-walled cylinder. Both graphitic (< 44 μm) and ultrafine diamond (~5 nm) powder were used, yielding deformation patterns that were radically different. Whereas the Ti-diamond mixture showed profuse localization upon being deformed to a effective strain of 0.38, the Ti-graphite mixture only exhibited embryonic shear bands. The shear localization regions showed the initiation of reaction in Ti-diamond mixture. For the Ti-graphite mixture, reaction was also observed in some isolated circular regions.

1. INTRODUCTION

The initiation of chemical reactions in condensed mixtures of energetic materials, such as Ni-Al, Ti-Si, Ti-C, Nb-Si etc., has been studied under dynamic plastic deformation [1-3] and shock loading [4-8]. It was demonstrated that different mixtures behave qualitatively differently under the same loading conditions. It was also shown [1] that mechanical instability (shear localization) was a necessary condition to initiate reaction

during dynamic plastic deformation. This is why the mechanical behavior of reactive materials during plastic flow (in inert state) plays a very important role in the initiation of chemical reaction. For example, chemical reaction is observed only inside shear bands in the Nb-Si mixture; in the Ti-Si mixture, under the same conditions, reaction was initiated inside shear bands and was able to propagate through the bulk materials [9].

The mechanical behavior can be changed by appropriate selection of mechanical properties of the mixture constituents, their porosity, morphology and phase content. For example, Nesterenko and Pershin [10] demonstrated that the addition of a plastic material (Cu, Ni) to a Fe-based amorphous powder decreased the degree of localized deformation in comparison with the one-component amorphous powder. For granular materials (ceramics, alumina [11] or silicon carbide [12]), instability of plastic flow and parameters of localized deformation depend on the initial particle size and initial porosity.

The effects of differences in mechanical behavior and initiation of chemical reaction between Ti-graphite and Ti-ultrafine diamond mixtures (at the same weight content and under dynamic plastic deformation conditions) are reported herein. The "Thick-Walled Cylinder" method developed by Nesterenko et al. [13,14] was applied using the same overall parameters of loading as previous reports for Ti-Si and Nb-Si mixtures [1,9].

2. EXPERIMENTAL TECHNIQUE

Ti-C (80 wt% - 20 wt%) powder mixtures in the stoichiometric composition of compound TiC were used in this research. The enthalpy of reaction ΔH is [15]:

$$Ti + C \rightarrow TiC \qquad \Delta H = -184.5 \text{ kJ/mole}$$

The Ti and graphite powders (from CERAC) had sizes of -325 mesh (< 44 μm), high purity (>99.5%) and irregular shape. Initial density of Ti-graphite mixture was 1.13 g/cm^3, and the initial density of Ti-diamond mixture was 1.5 g/cm^3. Ultrafine diamond

powder was produced by detonation synthesis and was chemically purified to provide a diamond content ~96% with particle size ~5 nm [17].

The thick-walled cylinder method was developed by Nesterenko et. al. [14, 15] for the investigation of high-strain, high-strain rate deformation of solid materials and modified for the study of inert [11] and reactive [1,9] porous powder mixtures. The schematic of the set-up is shown in Figure 1. Detonation is initiated at the top of the charge and propagates along the cylinder axis. The powder is first consolidated by a low detonation velocity explosive charge, which ensures the absence of chemical reaction at this stage. An orifice is then drilled along the cylinder axis and a second explosive event with higher detonation velocity is carried out. This second explosive produces significant plastic deformation in the densified powder layer. The velocity of the inner cylinder surface and the collapse time were measured by a noncontact electromagnetic method [14].

The details of the experimental configurations used to generate controlled strain and shear localization in porous samples are shown in Figure 2. A porous powder was initially placed in a tubular cavity between a central copper rod (diameter ~16 mm) and an outer copper tube (inner diameter ~20 mm and outer diameter ~31 mm). Explosive 1 (mixture of ammonite and sand in 3:1 volume ratio, Figure 2 (a)) with low detonation velocity (3.2 km/s) was used to densify the powder. No significant shear localization was observed after this stage because the global deformation is too small. This stage produced mainly the densification of the powder. Since the outer radius could be measured and were equal to 8.8 mm for Ti-graphite mixture and to 9 mm for Ti-diamond, the densities after this stage can be evaluated and are equal to 3.03 and 2.39 g/cm^3, respectively (Table 1). A cylindrical hole with diameter 11 mm was drilled along the longitudinal axis of the copper rod and this composite cylinder was collapsed by the detonation of a second cylindrical explosive charge (ammonite, Figure 2 (b)) with a detonation velocity of 4.0 km/sec, an initial density of 1 g/cm^3, and an outer diameter of 60 mm. This explosive 2 produced significant plastic deformation in the densified Ti-diamond mixture which was highly

localized in shear bands and not homogeneously distributed (Figure 2 (c) and Figure 3 (a)). In contrast, shear localization was much less developed in the Ti-graphite mixture (Figure 3(b)).

The global material strain can be obtained quantitatively from the strains in the incompressible copper shell driving the collapse process [14]. The radial and tangential true strains (ε_{rr} and $\varepsilon_{\varphi\varphi}$) and effective strains (ε_{eff}) for Ti-C system were calculated according to equations:

$$\varepsilon_{rr} = -\varepsilon_{\varphi\varphi} = \ln\left(\frac{r_i}{r_f}\right) \tag{1}$$

$$\varepsilon_{eff} = \frac{2}{\sqrt{3}}\varepsilon_{rr} \tag{2}$$

where the r_i and r_f are the initial and final radii. The data are presented in Table 2.

The state of stresses in these plane - strain experiments is very difficult to control, because during plastic flow they are determined by the material strength and its dependence on temperature, strain, and strain rate. Nevertheless, two main features of this method can mentioned:

(i) The weak shock waves propagating in materials during the first stage of collapse have no noticeable influence on the chemical reaction; their amplitudes are less than 1 GPa.

(ii) The superimposed "hydrostatic" pressure inside the collapsing incompressible cylinder [2] as a result of its acceleration toward the center is less than 0.1 GPa.

Thus, it can be concluded that pressure effects can be neglected to a first approximation and chemical processes are mainly strain controlled.

3. RESULTS AND DISCUSSION

Two different structures of carbon powders were mixed with Ti: ultrafine diamond and graphite. Under the same experimental conditions, profuse shear localization was observed in Ti - diamond mixture, but not in Ti - graphite mixture , as shown in Figure 3. However, the global strain is larger in Ti - graphite (ε_{eff} = 0.31~0.41) than in Ti - diamond (ε_{eff} = 0.26~0.35). The reason is that the Ti-diamond mixture did not change its density during deformation in contrast with additional densification in the Ti-graphite mixture during plastic flow. In the Ti-diamond mixture, the diamond is a hard and nondeformable component, transferring the deformation to titanium particles. Solid titanium itself is susceptible to shear localization at effective strains equal 0.3~0.5 [17]. On the other hand, graphite has a structure which can deform easily and uniformly. It resists the formation of shear localization regions macroscopically, uniformly accommodating plastic strains without essential plastic flow of Ti particles. This property of graphite results in a larger strain without global shear bands. Graphite is a lubricant and this property can also promote repacking of Ti particles without their plastic deformation.

The shear displacements, Δ, and shear band thicknesses, δ, for Ti - diamond are equal to 100~300 μm and 3 ~ 5 μm, respectively. Ti - graphite only shows embryonic shear bands. Figure 4 (a) shows one typical shear band structure with displacement, Δ, for Ti - diamond, compared to Figure 4 (b) for Ti - graphite. The local shear strains, γ (= Δ/δ), vary between 30~60 for the Ti - diamond mixture.

The microstructures of Ti - diamond and Ti - graphite mixtures are shown in Figures 5 and 6. A new networking structure is exhibited inside the shear bands (Figure

5). Diamond is a very inert material which cannot react easily [18]. However, diamond is not stable at low pressure and high temperatures and can undergo a structural change into graphite [19, 20]. The increase in temperature due to shear deformation work in the shear bands ($\Delta T_s = T - 300$ K) was estimated by Chen et al. [9]. The temperature inside shear band can be evaluated according to the equation:

$$T - 300 = \frac{1}{\rho C_p} \int_0^{\gamma} \tau d\gamma \qquad (3)$$

where T is the current temperature, ρ is the density, C_p is heat capacity, τ is shear stress and γ is shear strain. Taking the weight average heat capacity (C_p = 0.523 J/gK and 0.709 J/gK for Ti and diamond [21], respectively), the value is equal to 0.56 J/gK. From the Johnson-Cook equation, one can obtaine:

$$\tau = \tau_0 \left[1 + C \ln \frac{\dot{\gamma}}{\dot{\gamma}_0} \right] \left[1 - \frac{T - T_r}{T_m - T_r} \right]^m \qquad (4)$$

where γ_0 is reference strain rate T_r is reference temperature, and C is the strain rate sensitivity, m is the degree of thermal softening, T_m is the melting temperature and T is current temperature. A linear softening (m=1) and C = 1 [9] are assumed, and the melting temperature is taken as the weight average between Ti and C ($T_m \approx 2870$K). If the reference strain rate and temperature are taken as 1 s^{-1} and 300 K, and shear strength (τ_0) of solid Ti is equal to 280 MPa [17], the temperature as a function of local shear strain is obtained as:

$$T = 300 + \frac{1320\gamma}{1 + 0.51\gamma} \qquad (5)$$

Therefore, the temperature inside shear bands are equal to 2400~2800 K at γ = 30~60. It is clear that diamond is metastable in this condition and heat and shear deformation will accelerate its transformation to the stable graphite form. These results lead to the conclusion that Ti melted and diamond particles transformed into graphite inside shear

bands due to the heat generated by shear deformation work; this then leads to the initiation of reaction between molten Ti and graphite. The reaction can be facilitated by the increase of solubility of nanocrystalline carbon particles in Ti. This is confirmed by the chemical reaction of Ti-C powder mixtures, initiated with the onset of melting of Ti [22-24]. The porous structure is due to shrinkage because the reaction product, TiC, has a higher density than Ti and diamond. In comparison to the Ti-Si system [20], reaction cannot propagate in Ti - diamond system because the thermal conductivity of diamond is extremely high ($k \approx$ 1000 W/m.K [21]), which is ~50 times that of Ti; the large amount of heat loss restricts reaction propagation.

Unlike the Ti - diamond mixture, there was no significant shear band formation in Ti - graphite. Incipient shear localization was observed near the inner layer of the powder mixture. In these localized regions, the Ti particles were fractured and partially molten. The graphite particles reacted with Ti on the flow surface of Ti particles. This resulted in spherical reacted particle formation (shown by arrows in Figure 6 (c)) between or on the surfaces of fractured Ti. This is similar to the reaction products observed in previous investigations in the Ti-Si and Nb-Si mixtures [1, 2, 25]. LaSalvia et al.[26, 27] observed similar formation of spherules that result from the reaction between solid C and liquid Ti at the Ti-C interface.

4. CONCLUSIONS

(1) Shear bands are generated in Ti-diamond system, whereas larger homogeneous deformation is exhibited in Ti-graphite system, under the same experimental condition. This difference in response is due to the radically different mechanical response of diamond (hard) and graphite (a soft lubricant).

(2) The hard diamond forces the deformation to occur in titanium, which is known to be highly susceptible to shear localization. On the other hand, the soft graphite acts

as a lubricant between Ti particles which flow without plastic deformation. A schematic representation emphasizing the differences between the two Ti-C mixtures is shown in Figure 7. The graphite provides a lubricated layer between the Ti particles, which do not undergo significant plastic deformation. On the other hand, the diamond powders/agglomerates form a rigid "skeleton", and the plastic deformation is accommodated by Ti, which is known to be highly prevalent to shear localization.

(3) Chemical reaction is initiated between molten Ti and transformed graphite (from diamond) inside shear bands due to heat generated from shear deformation work in Ti-diamond system.

(4) Spherical reacted particles are observed in some isolated regions where shear localization occurred. In these regions, Ti particles underwent shear localization and partially melted, and then reacted with graphite.

ACKNOWLEDGMENTS

This research is supported by the U.S. Army Research Office, Contract DAAH04-96-1-0376 (Program Officer, Dr. E. Chen) and U.S. Office of Naval Research, Contract N00014-94-1-1040 (Program Officer, Dr. J. Goldwasser). The help of S. Usherenko with experiments is highly appreciated.

REFERENCES

1. V.F. NESTERENKO, M.A. MEYERS, H.C. CHEN, and J.C. LASALVIA, *Appl. Phys. Lett.*, **65** (24) (1994) 3069.
2. V.F. NESTERENKO, M.A. MEYERS, H.C. CHEN, and J.C. LASALVIA, *Metall. and Mater. Trans. A.*, **26** (1995) 2511.
3. J.J. DAVIS and D.L. WOODY, in Metall. and Mater. Applications of Shock-Wave and High-Strain-Rate Phenomena, eds. L.E. Murr, K.P. Staudhammer and M.A. Meyers, (Elsevier, 1995), p. 661.
4. B.R. KRUEGER, A.M. MUTZ, and I. VREELAND JR., *Metall. Trans.*, **23A** (1991) 55.
5. R.A. GRAHAM, "Solids under High Pressure Shock Compression: Mechanics, Physics, and Chemistry", (Springer-Verlag, New York, 1993).
6. N.N. THADHANI, *Prog. in Mater. Sci.*, **37** (1993) 117.
7. M.A. MEYERS, L.H. YU, and K.S. VECCHIO, *Acta Metall. Mater.*, **42** (1994) 715.
8. L.S. BENNETT, Y. HORIE, and M.M. HWANG, *J. Appl. Phys.*, **76** (1994) 3394.
9. H.C. CHEN, J.C. LASALVIA, V.F. NESTERENKO, and M.A. MEYERS, "Shear Localization and Chemical Reaction in High-Strain, High-Strain Rate Deformation of Ti-Si Powder Mixtures" (1997) in preparation.
10. V.F. NESTERENKO and S.A. PERSHIN, *Combustion, Explosion and Shock Waves*, **23** (5) (1987) 648.
11. V.F. NESTERENKO, M.A. MEYERS, and H.C. CHEN, *Acta Metall.*, **44** (5) (1996) 2017.
12. C.J. SHIH, V.F. NESTERENKO, and M.A. MEYERS, (1997) in preparation.

13. V.F. NESTERENKO, A.N. LAZARIDI, and S.A. PERSHIN, *Fiz. Goreniya Vzryva*, **25** (1989) 154 (in Russian).

14. V.F. NESTERENKO, M.P. BONDAR, and I.V. ERSHOV, in High-Pressure Science and Technology - 1993, eds., S.C. Schmidt, J.W. Shaner, G.A. Samara, and M. Ross, (Am. Inst. Phys., New York, 1994), p. 1172.

15. M.W. CHASE JR., C.A. DAVIES, J.R. DOWNEY JR., D.J. FRURIP, R.A. MCDONALD, and A.N. SYVERUD, "JANAF Thermochemical Tables, Third Edition, Part I, Al-Co." *Journal of Physical and Chemical Reference Data*, Vol. 14, 1985, Supplement No.1, American Chemical Society and American Institute of Physics for the National Bureau of Standards, 1986.

16. I. YU. MAL'KOV and V.M. TITOV, in Metall. and Mater. Applications of Shock-Wave and High-Strain-Rate Phenomena, eds. L.E. Murr, K.P. Staudhammer and M.A. Meyers, (Elsevier, 1995), p. 669.

17. V.F. NESTERENKO, M.A. MEYERS, and T. WRIGHT, *Acta Metall.* (1997) in press.

18. H. KUNISHIGE, Y. OYA, Y. FUKUYAMA, S. WATANABE, H. TAMURA, A.B. SAWAOKA, T. TANIGUCHI, and Y. HORIE, "Report of the Research Laboratory of Engineering Materials, Tokyo Institute of Technology", No. 15, (1990) 235.

19. H. LIANDER, *Industrial Diamond Review*, November (1980) 412.

20. A.B. SAWAOKA, M. TAKAMATSU, and T. AKASHI, *Adv. Mater.*, **6** (5) (1994) 346.

21. H.O. PIERSON, "Handbook of Carbon, Graphite, Diamond and Fullerenes - Properties, Processing and Applications", (Noyes Publications, New Jersey, 1993).

22. J.B. HOLT and Z.A. MUNIR, *J. Mater. Sci.*, **21** (1986) 251.

23. S.D. DUNMEAD, D.W. READEY, C.E. SEMLER, and J.B. HOLT, *J. Am. Ceram. Soc.*, **72** (1989) 2318.

24. J.H. LEE, N.N. THADHANI, and H.A. GREBE, *Metall. and Mater. Trans.*, **27A** (1996) 1749.

25 V.F. NESTERENKO, M.A. MEYERS, H.C. CHEN, and J.C. LASALVIA, in High-Pressure Science and Technology - 1995, eds., S.C. Schmidt and W.C. Tao, (Am. Inst. Phys., New York, 1996), p. 713.

26. J.C. LASALVIA, D.K. KIM, R.A. LIPSETT, and M.A. MEYERS, *Metall. and Mater. Trans.*, **26A** (1995) 3001.

27. J.C. LASALVIA and M.A. MEYERS, *Metall. and Mater. Trans.*, **26A** (1995) 3010.

FIGURE CAPTIONS

Figure 1. Schematic of set-up for thick-walled cylinder (TWC).

Figure 2. Geometry and sequence of deformation events in thick-walled cylinder method: (a) initial geometry, densified by explosive 1; (b) densified powder with central orifice cylinder collapsed by explosive 2; (c) final geometry.

Figure 3. Global view of profuse shear localization in Ti-diamond mixture and onset of instability in Ti graphite: (a) Ti-diamond mixture at $\varepsilon_{eff} \approx 0.35$; (b) Ti-graphite mixture at $\varepsilon_{eff} \approx 0.41$.

Figure 4. Comparison of shear localization in Ti-diamond and Ti-graphite mixtures: (a) a typical shear band structure with displacement, Δ, for Ti-diamond mixture at $\varepsilon_{eff} \approx 0.35$; (b) an embryonic shear band in Ti-graphite mixture at $\varepsilon_{eff} \approx 0.41$.

Figure 5. Microstructure of shear band in Ti-diamond mixture: (a) general view of the shear band; (b) higher magnification of the place shown by arrows in (a), which shows the networking structure.

Figure 6. Shear instability region in Ti-graphite mixture: (a) shear instability region near the inner boundary of powder mixture; (b) the reacted spherical particle along the unstable flows of the fractured Ti; (c) higher magnification which shows the reacted particle.

Figure 7 Schematic representation of differences in deformation between Ti-graphite and Ti-diamond.

Table 1 Experimental parameters in Ti-C mixture

Materials		Ti-diamond	Ti-graphite
Initial Radius (after Expl. 1)	r_0 (mm)	8	8
	r_{10}(mm)	9	8.8
Final Radius (after Expl. 2)	r (mm)	5.9	5.6
	r_1 (mm)	7.2	6.7
Initial Density (g/cm^3)		1.5	1.13
Density after expl. 1 (g/cm^3)		2.39	3.03
Theoretical Density (g/cm^3)		4.27	3.76

Table 2 Calculated global strain and shear-band spacing in Ti-C mixture

Materials		Ti-diamond	Ti-graphite
after explosive1	ε_{rr} ($-\varepsilon_{\varphi\varphi}$)	~0.10	~0.13
	ε_{eff}	~0.12	~0.15
after explosive2	ε_{rr} ($-\varepsilon_{\varphi\varphi}$)	0.22 ~ 0.30	0.27 ~ 0.36
	ε_{eff}	0.26 ~ 0.35	0.31 ~ 0.41
spacing between shear bands	L	~1 mm	-

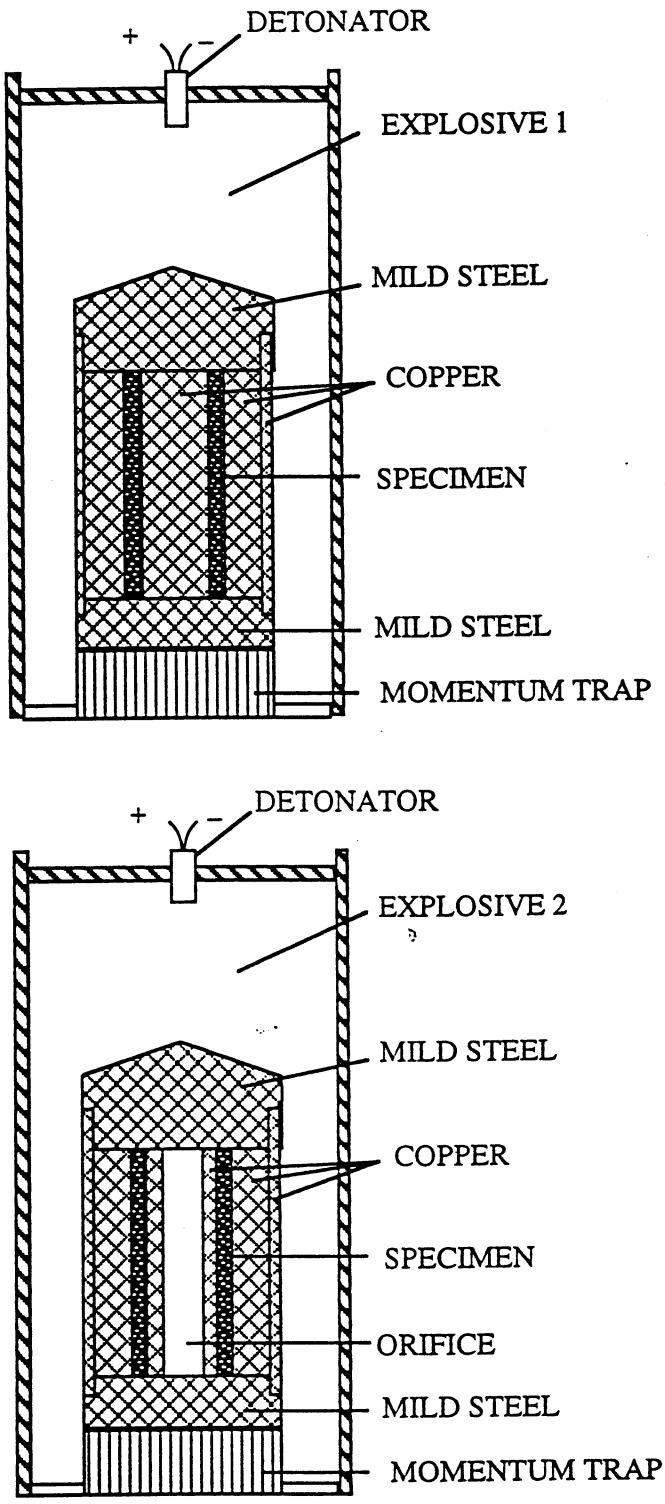

Figure 1. Schematic of set-up for thick-walled cylinder (TWC).

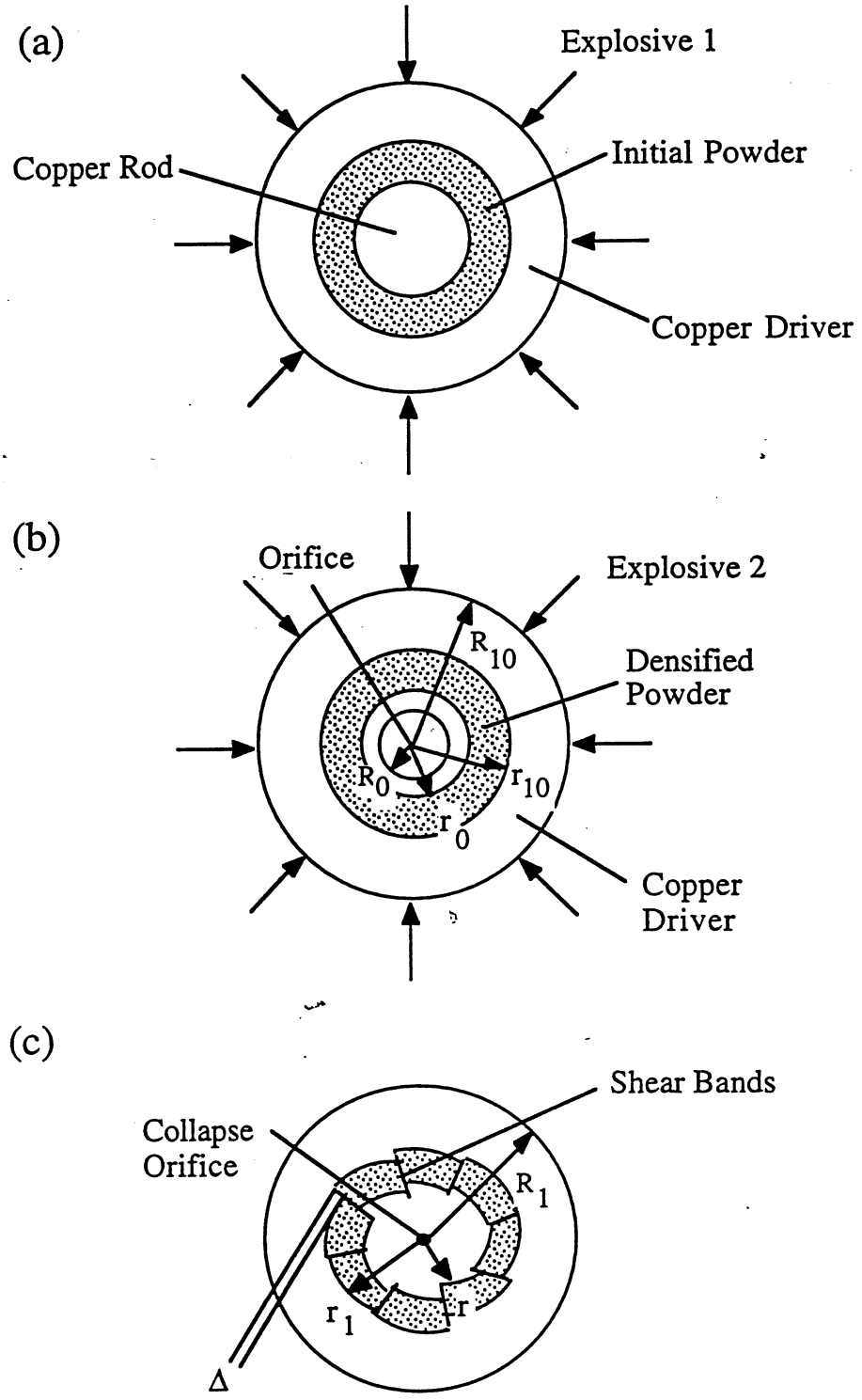

Figure 2. Geometry and sequence of deformation events in thick-walled cylinder method: (a) initial geometry, densified by explosive 1; (b) densified powder with central orifice cylinder collapsed by explosive 2; (c) final geometry.

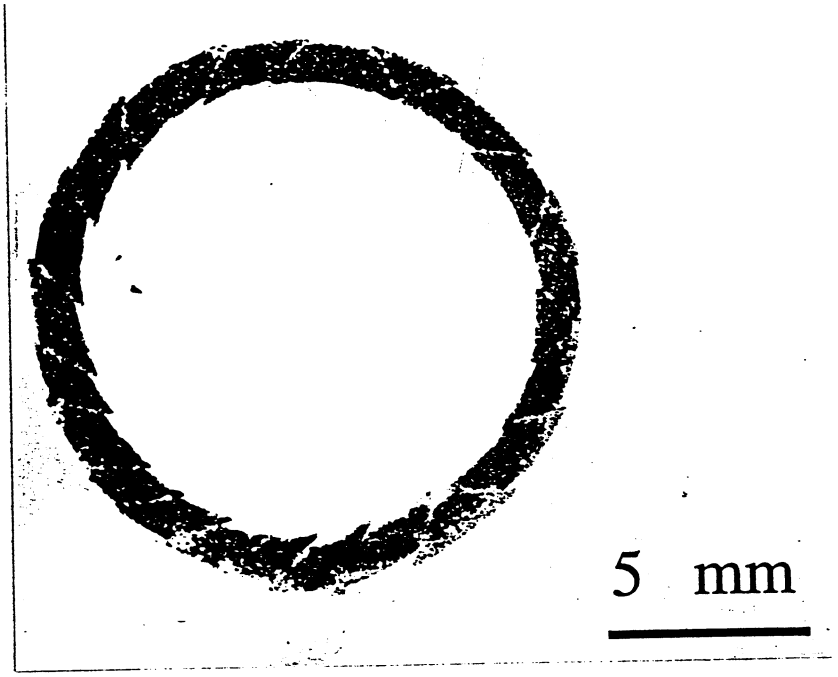

(a)

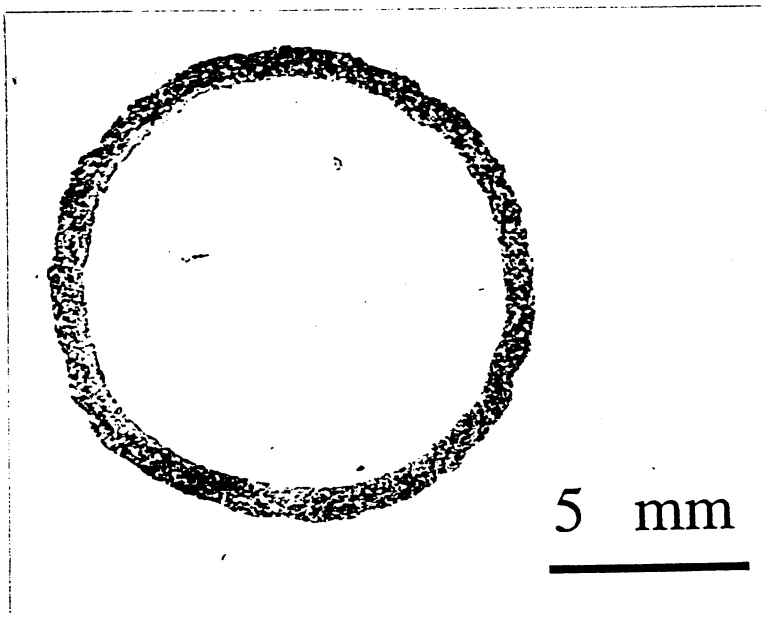

(b)

Figure 3. Global view of profuse shear localization in Ti-diamond mixture and onset of instability in Ti graphite: (a) Ti-diamond mixture at $\varepsilon_{eff} \approx 0.35$; (b) Ti-graphite mixture at $\varepsilon_{eff} \approx 0.41$.

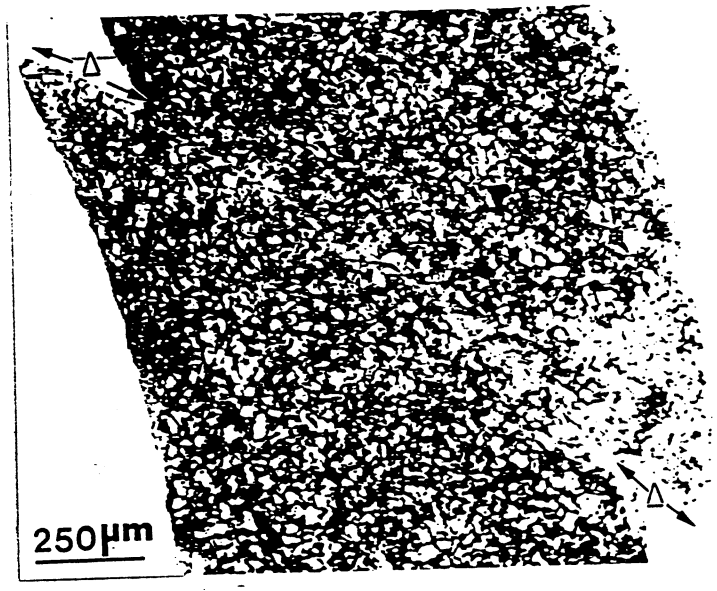

(a)

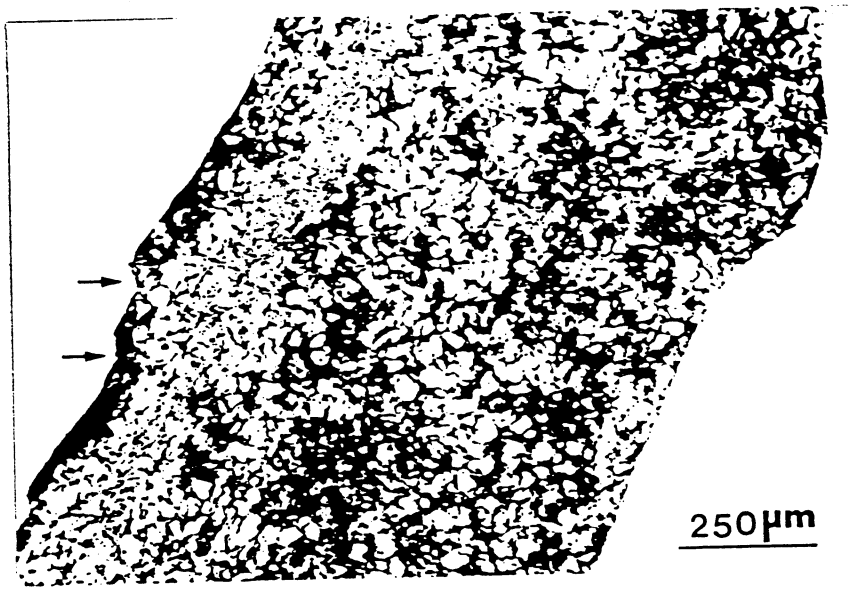

(b)

Figure 4. Comparison of shear localization in Ti-diamond and Ti-graphite mixtures: (a) a typical shear band structure with displacement, Δ, for Ti-diamond mixture at $\varepsilon_{eff} \approx 0.35$; (b) an embryonic shear band in Ti-graphite mixture at $\varepsilon_{eff} \approx 0.41$.

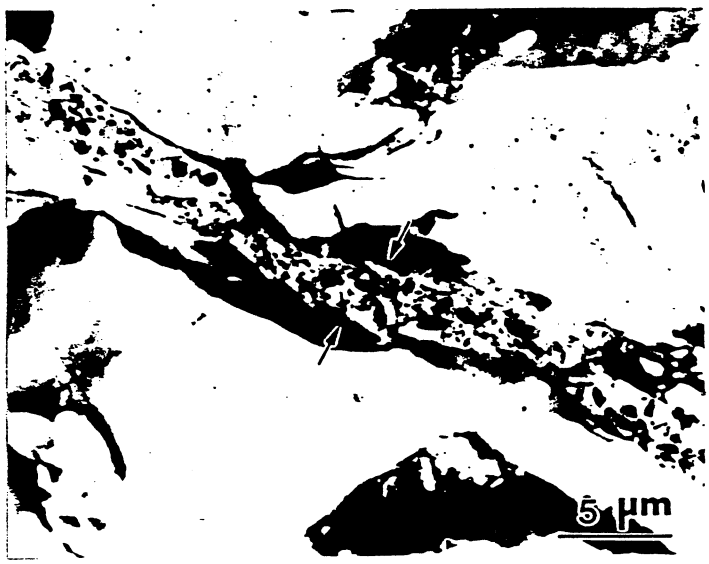

(a)

(b)

Figure 5. Microstructure of shear band in Ti-diamond mixture: (a) general view of the shear band; (b) higher magnification of the place shown by arrows in (a), which shows the networking structure.

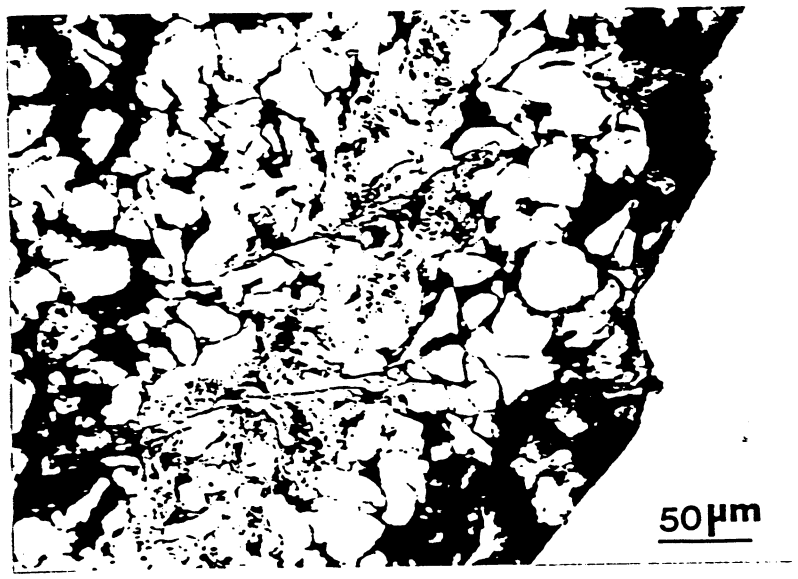

(a)

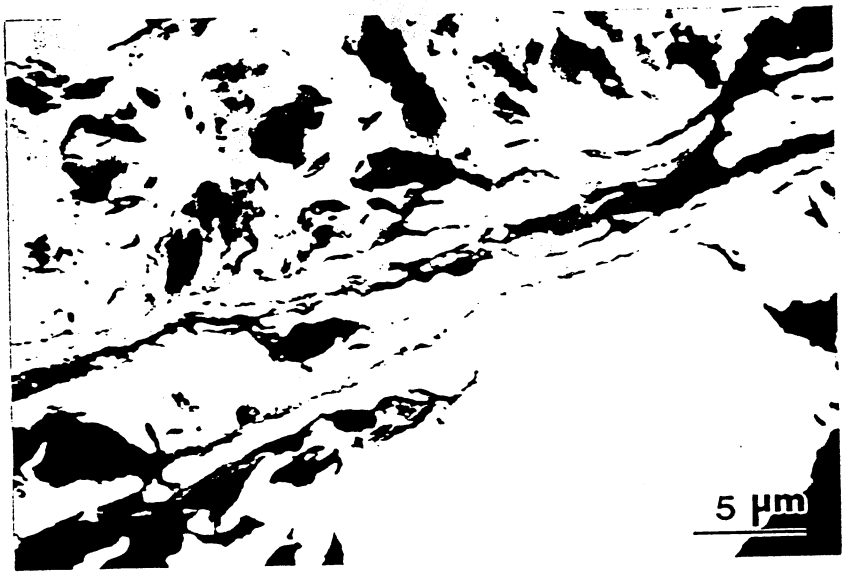

(b)

Figure 6. Shear instability region in Ti-graphite mixture: (a) shear instability region near the inner boundary of powder mixture; (b) reacted regions along the unstable flows of the fractured Ti;

(c)

Figure 6.(cont'd) (c) higher magnification which shows the reacted particles (see arrows).

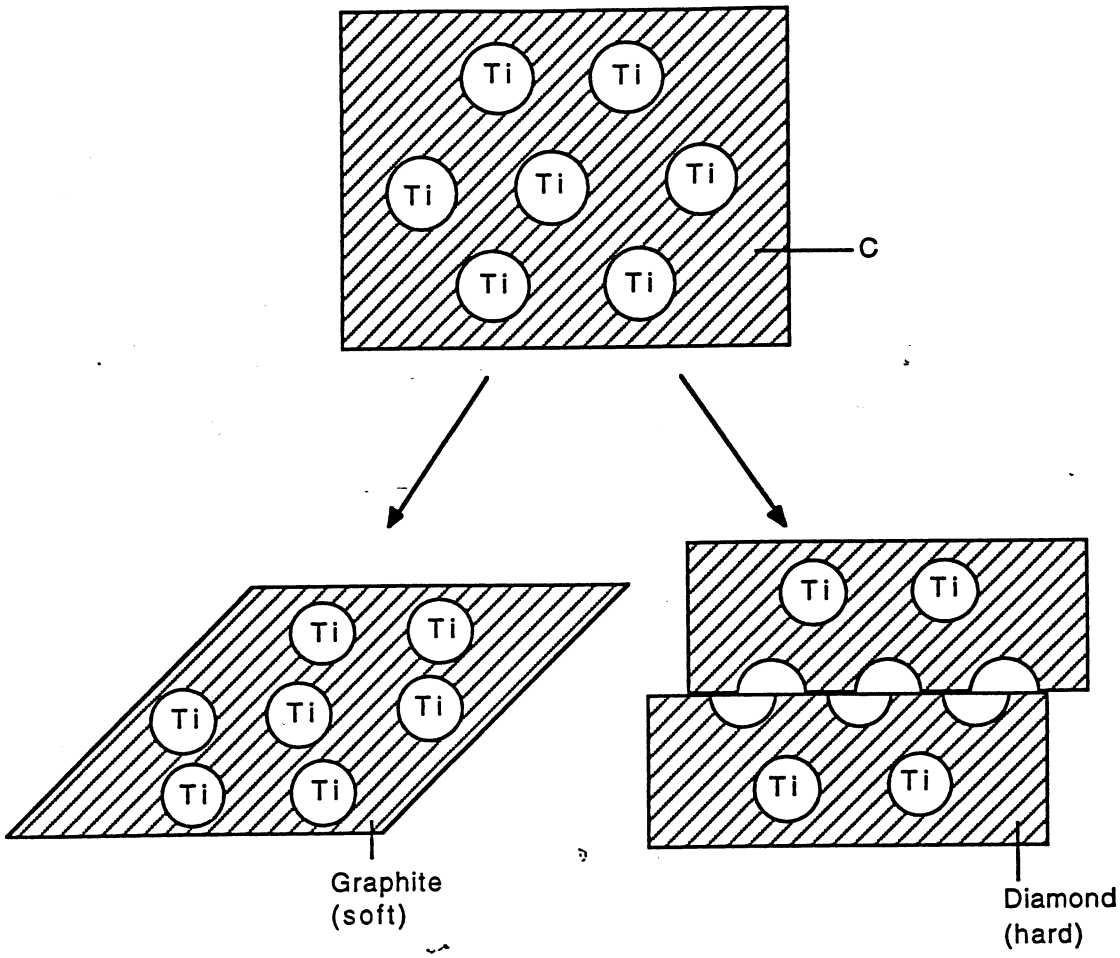

Figure 7 Schematic representation of differences in deformation between Ti-graphite and Ti-diamond.